JOURNAL OF MATERIALS SCIENCE 27 (1992) 6495–6505

Cold compaction of an aluminium/short fibre alumina powder composite

J. H. ter HAAR, J. DUSZCZYK
Laboratory of Materials Science, Delft University of Technology, Rotterdamseweg 137, 2628 AL, Delft, The Netherlands

Al–20 Si–3 Cu–1 Mg–0.3 Fe (wt%) rapidly solidified powder homogeneously mixed with 0, 5, 10 and 20 vol% Saffil alumina fibres, was subjected to cold uni-axial, single-action die-compression with progressively increasing pressures up to ~ 400 MPa and intermediate relaxation. The powders with 0 and 20 vol% fibres were also compacted to this target pressure in single steps and the resulting densification curves were compared to the progressive series curves. The densification behaviour during tapping (jolting) of the different powders was studied. Densification data were compared with two general and widely quoted compaction equations, being those due to Konopicky-Shapiro and to Kawakita. Above critical pressures, good agreement of experimental data with these relations was found. The tapping process of densification of the materials could be described by the Kawakita relation. The effect of both tapping and rigid-die compaction on fibre size was evaluated. Mean fibre size was not significantly affected by the tapping treatment. The extent of breakage during die compaction depended on the applied pressure.

1. Introduction

Metal matrix composites (MMCs) serve well to be produced using PM techniques because reinforcement in the powdered state can ideally be co-processed with matrix powder particles. The introduction of a hard (brittle) ceramic phase into a mass of, for example, relatively soft aluminium matrix powder particles, will result in a change of the bulk materials processing behaviour with respect to that of the pure matrix powder. This requires that the conventional PM processing route should be reassessed and newly optimized. PM processing of fully dense MMCs may consist of compaction by cold compression, degassing and working by extrusion, forging or rolling [1]. The extra step of mixing of PM MMCs practically appears to raise problems, basically due to the fineness of the particles involved [2–4]. The quality of the mix is of crucial importance because it will determine the quality of the final product to a large extent.

The quality of mixing depends on several factors such as the method used, particle types (composition), size difference, size distribution, shape, surface roughness and surface moisture content.

When a more or less homogeneous mixture of matrix and reinforcement has been obtained, preparations are needed to reduce the volume of the highly porous material, i.e. the material must be compacted. This is necessary for production, technical and economical reasons; the obligatory degassing treatment requires powders to be sealed in a cannister, while the volume of solid material produced per operation should preferentially be maximum.

Besides die-pressing, limited densification can also be attained by tapping or jolting (tap density) the powder in a container. This, however, will cause practically zero green strength as low-energy vibration involves no plastic deformation. For further consolidation, pressure should be applied to the powder.

The compactibility of a powder (the ease of compaction) will be affected by the presence of a second particle type. To control the amount of porosity and permeability and to conserve the size and size distribution in the special case of ceramic fibres, it is important to know the behaviour of such composited particle systems during compaction in order to extract the optimum processing conditions. The present investigation was performed to establish the influence of dispersed alumina fibres on the densification behaviour of a pre-alloyed aluminium powder. Densification by die compression of this composite material is applied as a pre-degassing step in which control of porosity (and permeability) is crucial for the efficiency of degassing.

An important factor which received attention was the fibre size during compaction. In general, with powder consolidation processes, it is economical to start with a high particle packing efficiency: late-stage porosity is eliminated only at the cost of high energy. However, normal cold-presssing applied to a fibre composite to improve initial packing is likely to cause extensive fibre breakage due to low contact-point numbers and high differential displacements.

2. Experimental procedure

2.1. Materials

The powders used in this study are air-atomized pre-alloyed aluminium with 20 wt% Si, 3 wt% Cu and

0022–2461

1 wt % Mg mixed with 5, 10 and 20 vol % aluminium oxide fibres (Saffil alumina RF type). The mixing was performed by dry ball-milling in a horizontal tumbler mill and led to a considerable fibre length reduction, resulting in shorter fibres for the higher volume fractions due to the necessity of applying longer mixing times [4, 5].

The rapidly solidified aluminium particles were rounded, irregularly shaped and had a rough surface resulting in a high specific surface area of $\sim 0.18\ m^2\ g^{-1}$. The powder has a wide particle-size distribution with a geometric mean size of 26 μm and a geometric standard deviation of the distribution of 2.1 (dimensionless) [4].

The alumina fibres are cylindrically shaped with a mean diameter of 3 μm. The distribution of lengths in the three composites can be described by log normal relations with geometric means (and standard deviations) of 38 μm (2.1), 30 μm (1.9) and 25 μm (1.8) [4, 5], respectively, for the powders with 5, 10 and 20 vol % fibres. An example of the powder mixed with 20 vol % fibres is presented in Fig. 1.

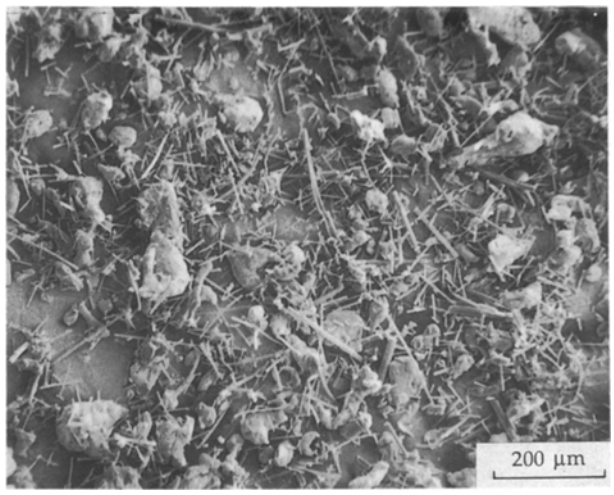

Figure 1 Scanning electron micrograph of a sample of the powder composite with 20 vol % alumina fibres.

2.2. Methods

Two important properties of powders are the apparent and the tap densities. According to ASTM standards, the apparent density is a density value of a loosely packed powder determined by a specified method. Likewise, the tap density is that density which can be attained by tapping or vibrating a mass of powder, again with reference to the method used. Because of bad flowability of the present mixed powders and the risk of segregation, the standard test method for determination of apparent density could not be used. Instead, an approximation of (relative) apparent density, D_a, was obtained by measuring column heights of the loose powders in the lubricated steel die.

Tap density of the powders (relative tap density, D_t) was determined and the densification behaviour with tapping number was studied with a STAV2003 JEL jolting volumeter. This apparatus consists of a 250 ml glass measuring cylinder placed on a machine which causes the glass/mounting clamp (675 ± 45 g) to jolt at $250 \pm 15\ min^{-1}$ with an amplitude of 3 ± 0.1 mm. Quantities of ~ 200 ml powder were inserted into the measuring glass by feeding it through a sharp-angled paper funnel. After distinct tap interval numbers the volume was read. The final tap volume and tap density were taken at the tap numbers where obliqueness of the powder level was preventing accurate read-out.

The mixed powders, as well as the unreinforced powder, were compacted by single-action uniaxial pressing in a steel die of 29.6 mm internal diameter. The powders were fed to the die through a sharp-angled paper funnel. To lower the friction with the die wall and piston head, a water-based graphite spray was used. Powder fill was such that the height to diameter ratio, H/D, of the compact was less than 1 to ensure a sufficiently high pressure transfer throughout the compact, in that way avoiding excessively high density gradients. Compact heights were measured from the piston relative to die displacements (at zero imposed load). A 0.3 MN hydraulic press was used with loads giving compacting pressures, P of 50.9, 76.3, 101.7, 203.5, 305.2 and 406.9 MPa. Two sets of experiments were performed. The first set (referred to below as PC series) involved progressively applying the above pressures to each compact, going repeatedly through the loading and unloading stages. In each case, the pressure was slowly increased to the target value where it was held for 15 s. After this six-stepped compaction, the compact was ejected. The second set of experiments (referred to as SC series) was only performed with the matrix powder and the composite with 20 vol % Al_2O_3 fibres and comprised filling of the die, slowly raising the pressure to one of the target values above, keeping it there for 15 s, measuring the compact height at zero load and finally ejection of the compact.

3. Theory

3.1. Introduction

Powders with a particle size < 500 μm generally have low densities due to inefficient packing [6]. The density of these particulate materials can often be increased by tapping or vibration. The energy barrier for this densification is due to mechanical interlocking and contact friction effects. The latter are more effective for small particles due to their high specific surface. During vibration treatments, the amount of interparticle space is reduced by the rearrangement of particles into better packing configurations. This is made possible by the temporary dilatations and consequent lowering of interparticle friction. The packing and rearrangement behaviour and with that, the evolution of porosity, depend on type, morphology and surface properties of the powder particles. The final density after a tapping or vibration treatment is also a function of the material, vibration amplitude, vibration direction, frequency, shear and test apparatus.

Consolidation of powders is usually performed by applying pressure to a constricted mass of powder,

frequently in combination with elevated temperature (uni-, bi-axial compression, cold or hot isostatic compression, pressure sintering). The compression can be static or dynamic, in the first case of which a powder is slowly loaded and held at a specific load for some time, the latter case comprising the transmission of several shock (pressure) waves through the powder.

During compression of a metal powder, pores are eliminated by particle rearrangement and particle shape change. The latter occurs through elastic deformation, plastic deformation or cracking. A powder consisting of a mixture of soft deforming (work hardening) and hard non-deforming particles will consolidate less easily because with less matrix volume a larger material strain is needed for the same amount of macroscopical compaction strain. Singh [7] has argued that in the case of a metal powder with inclusions of ceramic particles, the relative size of the two particle types in combination with their volume fraction is important in determining the compactability. In a study on compaction of metal powders with steel inclusions, Lange *et al.* [8] presented evidence indicating that the hard inclusions are constraining the matrix deformation above volume fractions of 0.20 through the formation of inclusion networks supporting a portion of the applied stress.

In the past, several attempts have been made to model mathematically the densification behaviour of metal, ceramic and pharmaceutical powders under an applied load or in tapping/vibrating compaction. Most of these models comprise empirically derived equations [9]. Some models exist which are valid only within limited pressure/porosity intervals. A very limited amount of work has been done on the densification behaviour of metal–ceramic powder mixtures.

Two widely used compaction equations which satisfy the theoretical boundary conditions (for $P = 0$ and $P \rightarrow \infty$) are treated below. One of them is the Konopicky-Shapiro equation [10] for compaction of metal powders. This equation can be looked upon as derived from the following differential equation putting the relative density change with pressure proportional to the fraction of pores

$$\frac{dD}{dP} = -\frac{dn}{dP} = K(1 - D) = Kn \qquad (1)$$

where D is the relative density, P the pressure, n the porosity, and K a material constant. The solution of Equation 1 gives the Konopicky-Shapiro relationship

$$\ln\left(\frac{1}{1 - D}\right) = KP + A \qquad (2)$$

It is noted that this equation is a description of the compaction process with no physical background. It appears to be applicable to metal powder compaction in the pressure range $\sim$ 100–700 MPa, i.e. at pressures above the range where a high proportion of particle rearrangement is thought to occur. The extent to which Equation 2 is valid for metal powders with a wide distribution of particle sizes, is not known. Most publications on this subject are concerned with comparison to theoretical compaction equations (except [11]) of compaction data from screened (sieved) powders.

When experimental metal powder compaction data are plotted on a logarithmic density scale versus P, it is often found that two different slopes can be recognized within different pressure ranges. From Equation 2, two different slope factors, K_1 and K_2, can be designated for these regions. The first slope factor, K_1, has been shown to be inversely proportional to the yield stress of the powder. Above a critical pressure the rate of densification can be expressed by a second slope, K_2, which appears to be directly related to the work-hardening capacity of the powders [10]. This critical pressure for some copper, iron and steel powders is reported to be around the value of 400 MPa [9]. Equation 2 is equivalent to Athy's equation [9], describing porosity

$$n = n_0 \exp(-K_3 P) \qquad (3)$$

where n is porosity, n_0 initial porosity, and K_3 a material constant.

The second widely used compaction equation is that of Kawakita. It is a very general equation used to describe the compaction of many kinds of powders:

$$C = \left(\frac{V_0 - V}{V_0}\right) = \frac{abP}{1 + bP} \qquad (4)$$

where C is the degree of volume reduction, V_0 the initial volume, V the volume under applied pressure, and a, b are constants characteristic of the powder. The constant a is equal to the initial porosity, whereas b is related to the forces resisting compaction [8]. No clear relationship between b and the physical properties of powders has been found. Equation 4 is usually rewritten as

$$\frac{P}{C} = \frac{1}{ab} + \frac{P}{a} \qquad (5)$$

The compression equation of Kawakita can also be applied to tapping (suffix T) and vibrating compaction [9]. For tapping compaction, Equation 5 transforms to

$$\frac{N}{C_T} = \frac{1}{a_T b_T} + \frac{N}{a_T} \qquad (6)$$

where N is the tapping number, C_T the degree of volume reduction and a_T and b_T are constants characteristic of the powder.

Another equation used to describe tapping compaction is that of Kuno [9]

$$(D_f - D) = (D_f - D_0)\exp(-K_4 N) \qquad (7)$$

where D_f is the relative density after infinite tapping number, D the relative density after a tapping number of N, and D_0 the initial relative density. It can be seen that this equation has the same form as Athy's Equation 3 for compression, and that because Equation 2 is identical to Equation 3, Equation 7 is similar in form to the Konopicky-Shapiro solution for powder compression.

In comparing the Kawakita equation (Equation 6) with Kuno's tapping equation (Equation 7) found a proportionality between the constant b_T in the first and the constant K_4 (ease of compression) in the latter equation can be found. The constant b_T was therefore considered to be related to the magnitude of cohesive forces between the powder particles [9].

In conclusion it can be said that the equations mentioned above should be regarded as giving very general descriptions, taking into account the fact that both can be applied to compression as well as tapping/vibrating compaction. Constants derived from fits should be interpreted with care. The Konopicky-Shapiro equation has empirically been proven to be valid only in a specific pressure range during metal powder compaction, whereas Kawakita is applicable to nearly the whole pressure range on any type of powder, indicating the more general nature of the latter.

In the next chapter, the results of our investigation into the compaction of the aluminium matrix composite powders will be described and the applicability of the model equations will be discussed.

4. Results

4.1. Tapping compactibility

Curves showing the densification behaviour of the powders during tapping compaction are presented in Fig. 2. The relative densities are plotted with their two-sided read-off errors (excluded for the 5 and 10 vol % data for the sake of clarity). These compaction curves can be seen as composed of two different stages separated by a discontinuity, each containing a concave and a straight section. It is noted that the densities at these discontinuities are approximately equal to the apparent densities as measured (see below).

The first stage will partly represent the process of elimination of the large macroscopic pores stemming from bridging particle masses. The concavity is an effect arising from the logarithmically scaled ordinate and the exhaustion of this process. Passing through this first stage requires higher tapping numbers for powders with higher fibre content, the end of this stage occurring at the discontinuity points of $N = \sim 20$, ~ 50, ~ 60 and ~ 90 for powders with fibre volume fractions of 0, 5, 10 and 20 vol % respectively. As expected, the composites with the higher volume of fibres show more difficulty in eliminating this porosity.

The 0 and 20 vol % composites more quickly approach a final density than both those with 5 and 10 vol % fibres. The data points of the powders at tap numbers $N > 100$ have been redrawn in a diagram of N against N/C_T to check their agreement with the Kawakita relation, Equation 6 (Fig. 3). The data points fit the linear curves representing the Kawakita relation.

From the slopes, the constants a_T can be derived which, together with the measured apparent densities, are used to calculate model values of relative density at infinite tapping number, N (model tapping density).

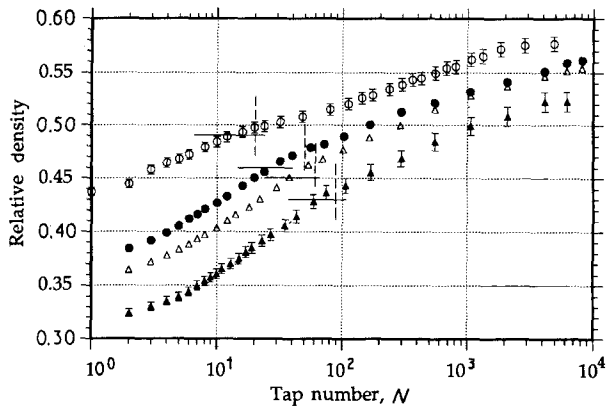

Figure 2 Relative density as a function of tapping number during tapping treatment of the powders. The two stages in each curve are separated by a vertical dashed line. Horizontal lines mark the apparent densities as measured V_f: (○) 0, (●) 0.05, (△) 0.10, (▲) 0.20.

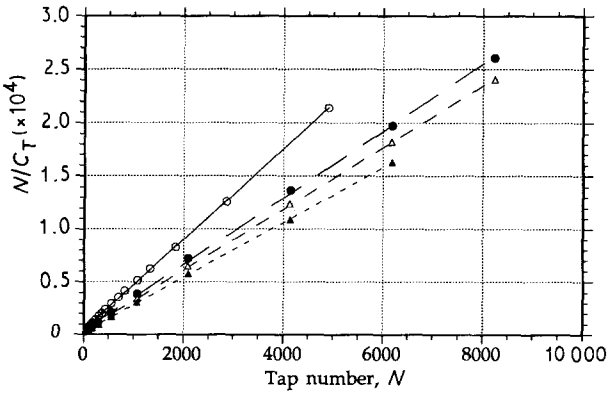

Figure 3 Kawakita plot illustrating the fit of the data points to the Kawakita equation for tapping compaction. V_f: (○) 0, (●) 0.05, (△) 0.10, (▲) 0.20.

From Equation 6 it is clear that

$$a_T = \frac{V_0 - V_\infty}{V_0} \tag{8}$$

where $V_{(N=\infty)} = V_\infty$ is the volume of material when $N \to \infty$. Because V_∞ is composed of two components

$$V_\infty = V_s + V_p \tag{9}$$

where V_s is the volume of solid, V_p is the volume of porosity at $N \to \infty$, Equation 8 can be rewritten as

$$a_T = (1 - D_0) - \left(\frac{V_p}{V_0}\right) \tag{10}$$

The quotient V_p/V_0 can be calculated because D_0 is known from experiment. The model density values $D_{(N=\infty)} = D_\infty$ are then obtained from

$$D_\infty = 1 - \frac{V_p}{V_0(1 - a_T)} \tag{11}$$

The constants a_T and b_T derived from Fig. 3 are listed in Table I. The values of D_∞ are given in Table II and are discussed below.

While for mono-solid equidimensionally shaped particulate material, b_T is connected with cohesive

TABLE I Constants a_T and b_T of Equation 6.

V_f	a_T	b_T
0	0.234	0.0095
0.05	0.318	0.0090
0.10	0.344	0.0108
0.20	0.384	0.0131

TABLE II Densities and Hausner ratios of the powders

V_f	D_a	D_t	D_∞	D_t/D_a
0	0.49	0.577	0.644	1.178
0.05	0.46	0.561	0.673	1.220
0.10	0.45	0.554	0.687	1.231
0.20	0.43	0.522	0.696	1.214

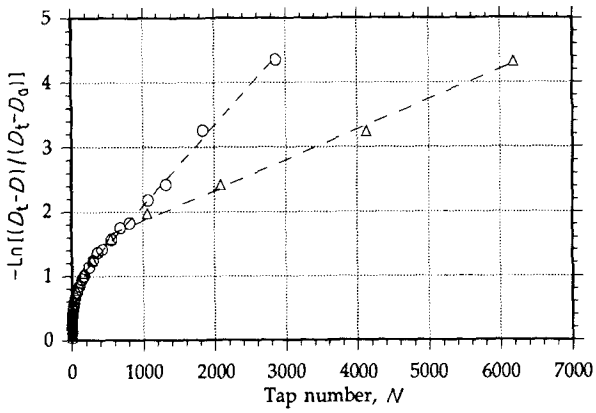

Figure 4 Illustration of limited compatibility to Kuno's tapping equation of tapping compaction data from powders with (○) 0 and (△) 10 vol % fibre reinforcement.

forces [9], in the present case of fibre composites it will more likely reflect an apparent degree of powder cohesivity due to geometrical locking. Looking at these values, it appears that the constant b_T is not significantly different for 0 and 5 vol % fibre content, but increases on increasing the fibre content to 10 and 20 vol %. When the density data are presented according to the Kuno equation (Equation 7) as N versus $-\ln[(D_f - D_N)/(D_f - D_0)]$, where D_f and D_0 are approached by D_t and D_a respectively (Table II), it appears that the exponential relationship is only valid at tap numbers N higher than ~ 200 in the case of the matrix powder, and at tap numbers N higher than ~ 500 in the case of the composite powders. Only data of the 10 vol % composite are given in Fig. 4. Because a large part of the initial consolidation will be due to the elimination of bridging porosity, these results strongly suggest that it is this mechanism that will be exhausted at tapping numbers $N \sim 200$ in the case of the matrix powder, and only at $N \sim 500$ for the three powder composites.

The tap and apparent densities (D_t and D_a, respectively) of the powders are listed in Table II. The latter are determined from initial column heights of loose powder in the compaction die. Both tap and apparent density decrease with increasing volume percentage of reinforcement. This is in accordance with the idea of a hindered optimal particle packing due to increased bridging and geometrical locking effects amongst the fibres and aluminium particles. The values D_∞ are calculated values of relative density at infinite tapping number by assuming that the Kawakita relation is valid for the whole range. Instead of decreasing, as does the measured tap density, the values of D_∞ increase with increasing fibre content. This indicates that the Kawakita relation does not model the densification of the present materials correctly in the range of high tapping numbers.

Hausner [12] has suggested that the quotient of tap and apparent density might be used to describe powder friction. Despite differences in fibre size and volume fraction, the ratios D_t/D_a for the present composite powders are all similar and higher than for the unmixed powder. However, Kostelnik and Beddow [13] proved that this so-called Hausner ratio is also very sensitive to particle size and shape. Moreover, it is difficult to interpret when dealing with powder mixtures. Grey and Beddow [14] showed that the ratio is more significant for the friction in a moving powder mass than for that in the static condition.

4.2. Pressing compactibility

Fig. 5a and b show the compaction curves of the matrix and the composite powders during compression. In the intermediate pressure range used (50–200 MPa) absolute densities increase with volume percentage of fibres. There appear to be only small differences in relative density between the different composites at pressures above 50 MPa (Fig. 5b).

In Fig. 6a and b the compaction curves of the 0 and 20 vol % powders from the two experimental series (PC and SC) are compared. It can be seen that the PC series experiments give slightly higher densities, the differences being of the same order of magnitude in the whole pressure range.

In Fig. 7, the powder compression data are represented in a diagram of P versus $\ln[1/(1 - D)]$ to visualize the validity of the Konopicky-Shapiro relation for P above 50 and 100 MPa for the matrix powder and the composites, respectively. It can be seen that only the pure matrix powder shows the linear relationship with pressure in accordance with the linear region which is usually described with a slope factor K_1. It is likely that the initial negatively deviating region in which a large share of particle rearrangement and restacking occurs, is extended towards higher pressures in the case of fibre composite powders.

In general, powder compression data plotted according to the Kawakita relation (Equation 4) as P/C versus P, frequently show a linearity except for the initial part of the curve (Fig. 8). From the slope of this line, the initial relative density should result because at $P = \infty$, $C_\infty = (V_0 - V_\infty)/V_0 = a = (1 - D_0)$. The values of a derived in this way are given in Fig. 9.

The values of $D_0 = (1 - a)$ do not change significantly with fibre volume fraction. The difference

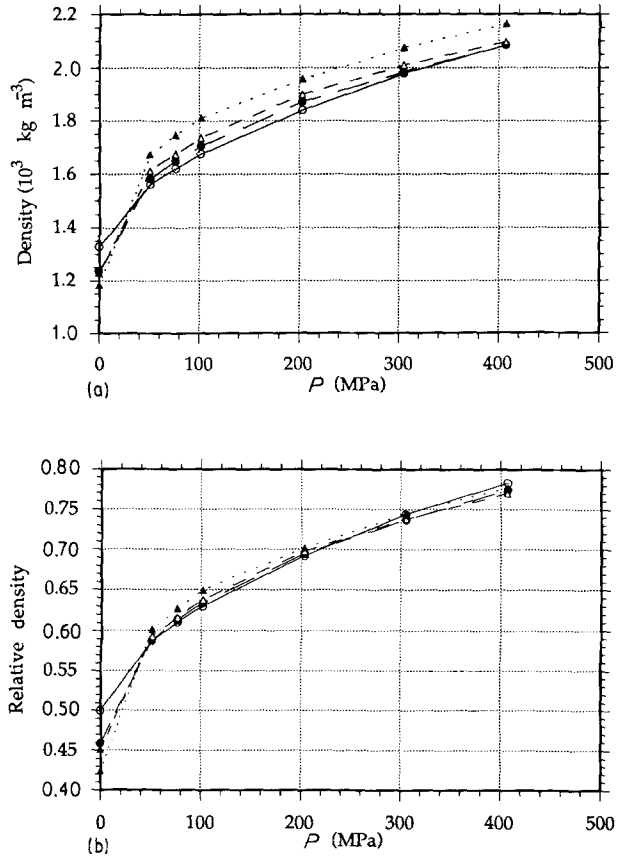

Figure 5 (a) Density and (b) relative density of die-pressed powders as a function of applied pressure. V_f: (○) 0, (●) 0.05, (△) 0.10, (▲) 0.20.

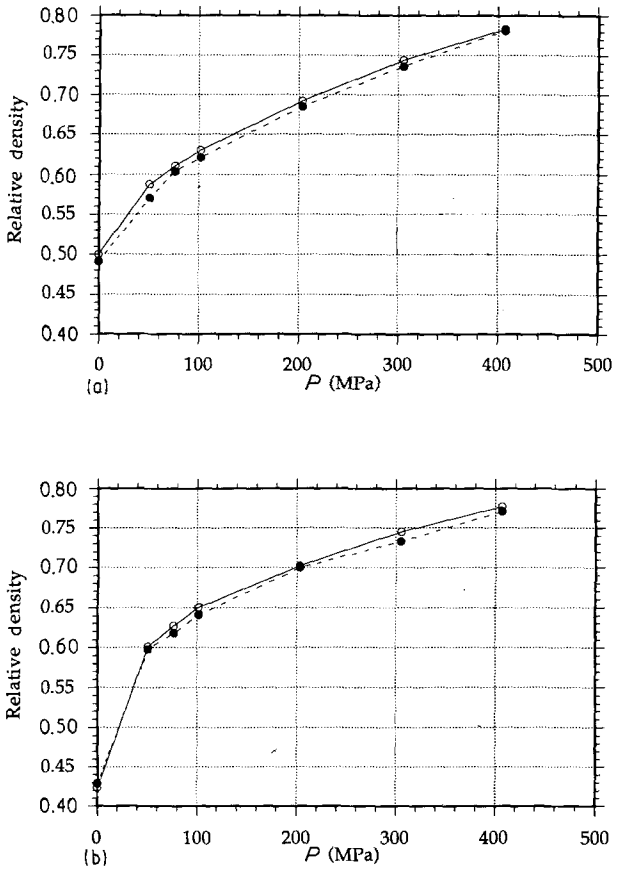

Figure 6 Comparison of (———) PC and (– – –) SC compaction curves for (a) 0 and (b) 20 vol % fibre-dispersed powders.

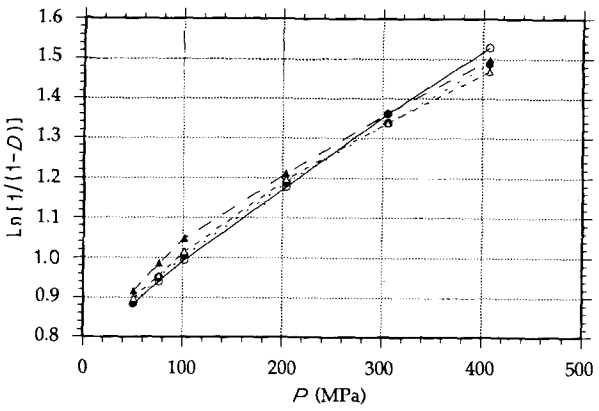

Figure 7 Plot of PC compaction data to illustrate the compatibility of behaviour of the powders with respect to the Konopicky-Shapiro relation: $\ln [1/(1 - D)] = KP + A$. V_f: (○) 0, (●) 0.05, (△) 0.10, (▲) 0.20.

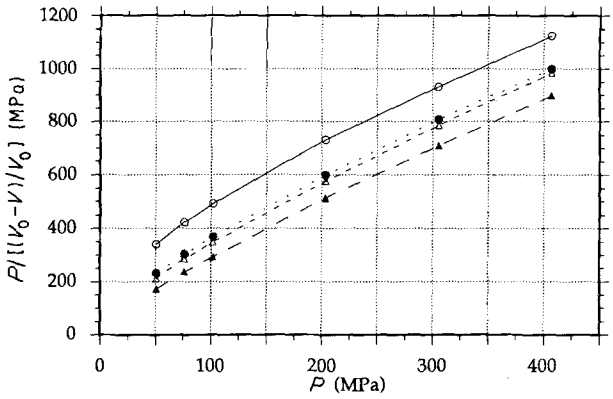

Figure 8 Plot of PC compaction data to illustrate the compatibility of behaviour of the powders with respect to the Kawakita relation: $P/C = (1/ab) + (P/a)$. V_f: (○) 0, (●) 0.05, (△) 0.10, (▲) 0.20.

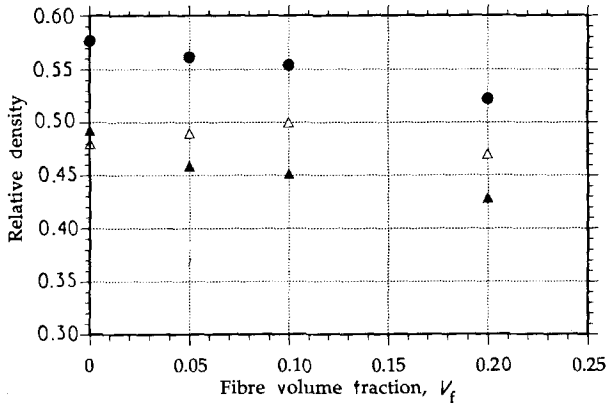

Figure 9 Tapping and apparent densities as a function of reinforcement volume fraction. Note that fibre size differs with volume fraction. (●) D_t, (△) Kawakita theory $D_0 = 1 - a$, (▲) D_a.

between the measured apparent density and the theoretical value $D_0 = (1 - a)$ is negligible for the pure powder and increases with higher volume fraction of fibres.

4.3. Comparison

Fig. 10a and b give the tapping and piston compression data for the powders with 0 and 20 vol % fibres in

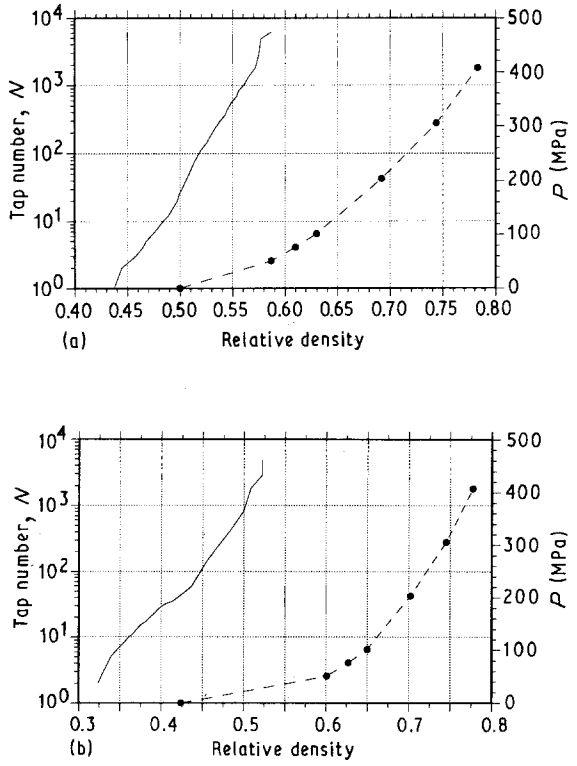

Figure 10 Comparison of green densities reached during tapping and die compression for (a) 0 and (b) 20 vol % fibre composite powders. Differences in initial densities are due to different filling conditions. (———) Tap number, N; (–●–) compacting pressure, P.

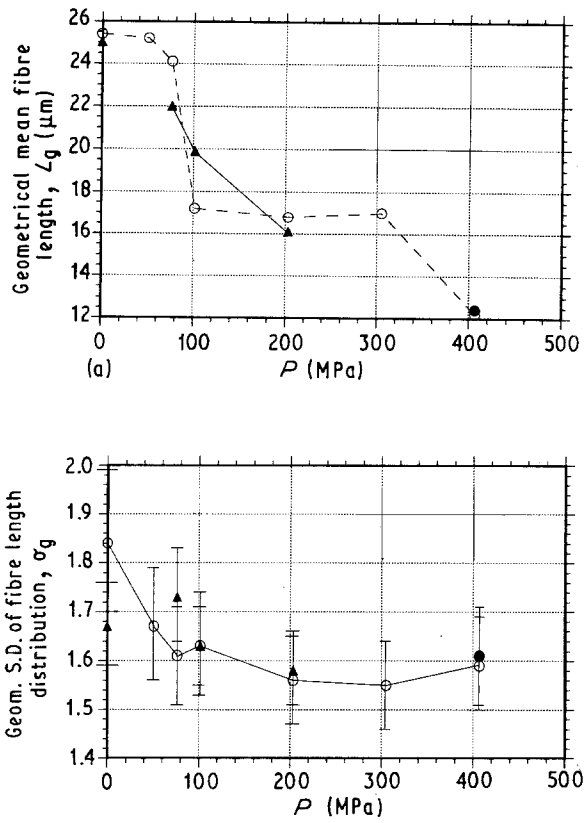

Figure 11 Results of microscopic fibre size analyses on samples of die-pressed compacts with 20 vol % fibres. (a) geometric mean fibre length, L_g, (b) geometric standard deviation, σ_g. (○) SC series, local; (●) PC series, local; (▲) SC series, global.

single diagrams of relative density. It is obvious that if a high green density and green strength are required for the compact, die compression will be necessary. With the (pre-) consolidation of metal/ceramic fibre dispersed powder for degassing purposes, the priorities are different. Because for canned compaction, high green strength is not required and because the fibres used are very brittle and prone to fracture, it seems undesirable to use die compression. In a case like this, provided that the batch solid volume of material to be processed is not critical, partial densification by tapping might provide a good alternative. The effectiveness of compaction by vibration can be increased by the use of higher vibrational frequencies (~ 80–500 Hz) [15].

4.4. Compaction damage to fibres

The compacts of the SC series with 20 vol % fibres have been subjected to a fibre length analysis. This material was chosen because it was expected that the most intense breakage would occur with the highest fibre loading. Small samples of the upper middle part of the compacts were taken, the matrix particles were dissolved and the lengths of ~ 110 fibres were measured with a light microscope. The geometric mean lengths are given in Fig. 11a. A large decrease in fibre length occurred in the loading range 75–100 MPa. The significance of this for a larger volume of the compact was checked by doing a second analysis and dissolving a larger volume from the internal part of the compacts. This time the analyses were performed by measuring ~ 200 fibres with an image analysis system connected to the microscope. These global analyses suggest that the decrease in fibre length with pressures up to 100 MPa is more continuous.

Fig. 11b gives the values of the geometrical standard deviation, σ_g, of the distributions of fibre length in the composites with 20 vol % fibres as a function of compaction pressure. σ_g is a dimensionless measure of the width of the distribution relative to the mean (Appendix 1); for a perfect lognormal distribution it is equal to the quotient of the 84 and 50 percentiles. The bars given in the figure are error intervals calculated with sample variance analysis (Appendix 3). It should be noted that the measurements represented by circles (local) have been performed using handcounting while the triangle data points represent semi automatic computer counting. From the first dataset (local) it can be concluded that the standard deviation of the fibre-size distribution (the relative width) has changed significantly at pressures of 200 MPa and higher. No firm conclusions can be drawn from this in the low-pressure range. The global fibre-length analyses do not present significant differences with respect to the local measurements.

Some of the measured distributions of fibre length in the composites were tested for lognormality after tapping and compression. The χ^2 test for analysis of variance (Appendix 2) is used for this purpose. It had already been found that measured lengths of fibres in the starting powders could be described by the lognormal distribution function [4]. The same test was applied again in the present classified size data and the

TABLE III Results of χ^2 tests on measured fibre length distributions

V_f	P (MPa)	Tapp. appl.	L_g (μm)	f	$\Sigma\chi^2$	$\chi^2(p = 0.05)$	H_0 acc.
0.05		–	38	13	12.72	22.36	+
0.05		+	37	14	17.61	23.69	+
0.10		–	28	12	20.28	21.03	+
0.10		+	28	12	25.67	21.03	–
0.20		–	25	13	14.19	22.36	+
0.20		+	26	11	22.89	19.68	–
Before/after compression, $V_f = 0.20$							
		–		10	14.76	18.31	+
	76			11	10.74	19.68	+
	102			9	11.08	16.92	+
	204			9	10.17	16.92	+

results are given in Table III. The data suggest that tapping applied to the composite powders causes some change in the fibre length distribution such that the $\Sigma\chi^2$ values (a measure of the deviation from log normality) increase. This occurs, however, without a significant change in the geometric mean length. The distributions of fibre length in the 10 and 20 vol % fibre composite powders as measured after tapping are such that the lognormality hypothesis is no longer accepted. However, due to errors involved in the standard deviation of the fibre length distribution (see Fig. 11b) it is not possible to draw firm conclusions concerning lognormality of the true distributions when the $\Sigma\chi^2$ values are so close to the tabulated 95% confidence limit (i.e. for $V_f = 0.10$ before tapping and $V_f = 0.20$ after tapping; Table III).

Fig. 12 shows the measured distribution (global) of fibre lengths in a 20 vol % fibre-reinforced powder compact. The ideal lognormal curve drawn with the calculated statistics from the distribution $L_g = 16$ μm and $\sigma_g = 1.58$ is also given. Table III presents the results of the χ^2 tests on some fibre distributions obtained after compressing the powder with 20 vol % fibres. It is found that the distribution of fibres can still legitimately be described by a lognormal function after compression at 204 MPa.

Fig. 13 shows the aggregate morphology of this very low-strength compact on a fracture surface. It should be noted that there is a large fraction of fine porosity in this material. Also it is recognized that very few (aluminium) particle–particle contacts occur in this material.

Describing the fibre length by a lognormal probability function and subtracting these distributions at compaction pressure, P from the original yields, after normalizing the graph shown in Fig. 14. It illustrates the cut-off length below which relative fibre numbers show a net increase and above which they show a net decrease. It is remarkable to find that this parameter is more or less the same (~ 21 μm) for the three pressures shown.

5. Discussion and conclusion

Compression of the composite powders with 5, 10 and 20 vol % fibres in the range 50–400 MPa does not yield significant differences in porosity level compared to the unmixed aluminium metal powder. It is deduced that the wide aluminium particle size distribution allows for the introduction of fibrous particulates without a large dilatation in the packing and that the

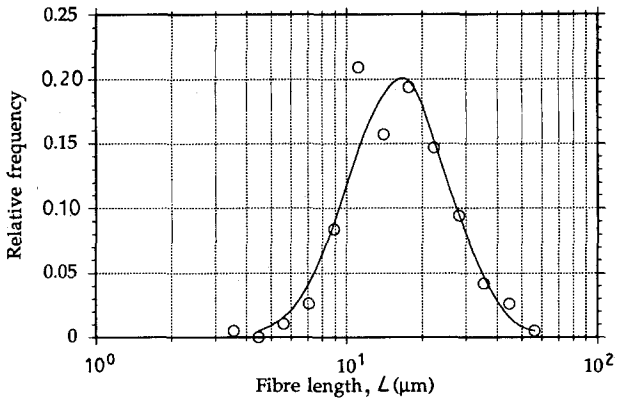

Figure 12 Fibre length distribution of the 20 vol % fibre composite as affected by die-pressing at 204 MPa. $L_g = 16$ μm, $\sigma_g = 1.58$. (○) Actual, (———) lognormal.

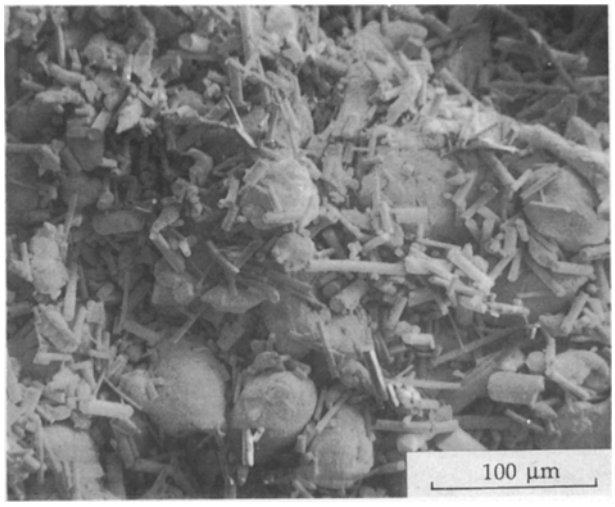

Figure 13 Scanning electron micrograph of fractured surface of a compact with 20 vol % fibres pressed at 203.5 MPa.

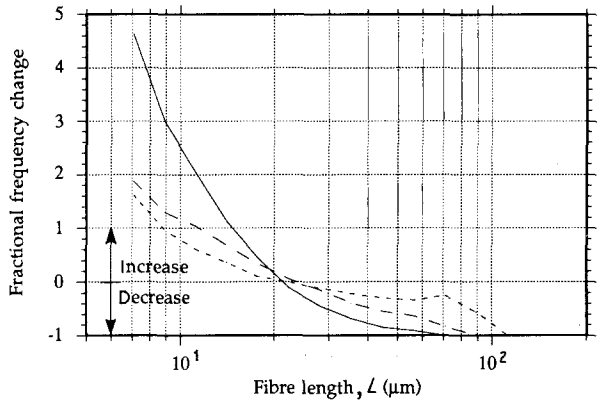

Figure 14 Graph illustrating the relation between the original fibre length distribution and those after compression of the 20 vol % fibre composite, at (———) 204 MPa, (– – –) 102 MPa and (----) 76 MPa.

fibres are easily fractured. With tapping (vibrating) compaction, larger differences in porosity level do exist, except between the 5 and 10 vol % composites at higher tapping numbers. Relative densities of 0.58, 0.56, 0.55 and 0.52 have been obtained in this way for 0, 5, 10 and 20 vol % fibre-dispersed powders, respectively.

Kawakita plots of the tapping compactibility data show good agreement with the theoretical relation for all powders at all applied tapping numbers. However, the limit densities, D_∞, predicted by the Kawakita relation are different from the tap density values as determined. The differences increase with fibre loading. The data fit the Kuno tapping equation at tapping numbers N higher than ~ 200 for the undispersed aluminium powder, and at tapping numbers N higher than ~ 500 for the composite powders.

When the pressure compactibility data are represented in a plot of $\ln [1/(1 - D)]$ versus P, the data of the pure matrix powder ($P > 50$ MPa) satisfies the Konopicky-Shapiro relation giving a straight line, while the composites show curved lines. In contrast to what is generally believed to be due to pure particle restacking, Hewitt *et al.* [11] have demonstrated that the first stage in compaction of their atomized iron powder also involves plastic deformation. A metallographical study [16] of the contact facets of bronze powder particles after compaction revealed that particle sliding proceeds well into the stage where plastic deformation occurs, up to relative densities of 0.8. The drawing of conclusions on compaction mechanisms on the basis of the present type data is very tricky. It is, however, reasonable to believe that the composites undergo a larger share of particle sliding during compaction as compared to the pure matrix powder which is, moreover, extending towards higher pressures. A transition of local to homogeneous plastic flow, coinciding with the transition to linearity in a plot of $\ln[1/(1 - D)]$ versus P, is likely to have occurred in the pure matrix powder whereas it is less likely for the composites. Additionally, it is noted that the matrix in the composites may exhibit a delayed plasticity because a portion of the applied consolidation pressure will be supported by the established fibre network [8].

Pressing compactibility data represented in a Kawakita plot of P/C versus P also show a negative deviation of linearity at pressures $P < 200$ MPa for all the powders, which is in agreement with literature data on compaction of metal and oxide powders [9]. The compaction data for $P > 200$ MPa could be fitted with straight lines for all powders in a Kawakita plot.

During die compaction of the composite powders, fibre breakage occurred. In the composite with 20 vol % fibres, the global geometric mean fibre length decreased from 25 μm to 22 μm when compressed at 76.3 MPa. After compression at 406.9 MPa, a geometric mean length of 12 μm was determined in the upper middle part of the billet. Tapping compaction, however, although not reaching as high densities, does not cause significant reduction of mean fibre size. With this result, the question arises as to whether the higher density obtained by die pressing, as opposed to tapping (vibrating) compaction, preferentially outweighs the contemporaneous decrease in fibre length. To answer this question one needs to know the fracture behaviour of the fibres during the processing stage of extrusion and its relation to initial packing and porosity.

It is argued that for the processing of fibre composites, it is beneficial to pass the initial stage of compaction by tapping such that much less damage to fibres is done in this stage. In this way the large consolidation pressures are not applied before a network of matrix particles, supporting a portion of the applied stress, is formed. Owing to the assumed small pore size and low connectivity in combination with the low mobility of the elongated fibres in the powder mix, large-scale segregation of particles will not occur during tapping.

Appendix 1. The log normal probability distribution

The log normal probability density function can be derived from that of the normal distribution by replacing the variable and the population statistics in the normal function definition by their logarithmic equivalents

$$f(x') = \frac{d\varphi}{dx'} = \frac{1}{\sigma'(2\pi)^{1/2}} \exp - \left[\frac{(x' - \mu')^2}{2(\sigma')^2}\right] \tag{A1}$$

with $x' = \log x$, $\mu' = \log \mu_g$, $\sigma' = \log \sigma_g$, where μ', μ_g are arithmetrical and geometrical population means (expectations) and σ', σ_g are arithmetrical and geometrical standard deviations. It is seen that σ' is the standard deviation of the logarithm of the variable ($\log x$) with respect to the expectation of $\log x$ ($\mu' = \log \mu_g$).

The ideal population statistics μ' and σ' can be approached by the values calculated from a measured sample data set through

$$\log \bar{x}_g = \log\left(\prod_i x_i^{\Delta\phi_i}\right)^{1/\phi} \tag{A2}$$

$$\log s_g = \left[\frac{\sum_i (\log x - \log \bar{x}_g)^2 \Delta\phi_i}{\phi}\right]^{1/2} \tag{A3}$$

with $\phi = \sum_i \Delta\phi_i$, where $\bar{x}_g$ is the geometrical sample mean, s_g is the geometrical sample standard deviation and $\Delta\phi_i$ is the frequency of class size (interval) i. When a variable is supposedly distributing lognormally, data processing and interpretation can be made easier by converting the values to their logarithms and treating them as distributing according to the normal law.

Appendix 2. Performing the χ^2 test

The χ^2 (chi-squared) test is a test involving the analysis of variance in a data set (e.g. a particle-size distribution) in order to make a clear statement on the occurrence of a certain event (e.g. normality of measured particle-size distribution). To do so, a measured

variance is compared with the probability of the variances in the ideal case of a true event. In the present case, the χ^2 test is applied to assess the goodness of fit between theoretical and observed particle-size distributions.

Of a number of n particles in a microscopic sample taken from a batch quantity of powder, the maximum particle dimension, l, in the plane of image is measured. The values of the variable were classified in intervals, l_i, with a logarithmic progression of class boundaries and class midths $l_{ai} = 10\exp(0.1 + k\ 0.05)$ with k EN $[1, \infty]$. With the logarithm of the class midth sizes and the class frequencies, the geometric mean and standard deviation were obtained. The normal deviate $(\log l_g - \log l_i)/\log \sigma_g$ is then calculated and the corresponding cumulative frequencies are transcribed from a statistic table. We arrive at the theoretical frequencies by multiplication of the relative frequencies and the sample size. The test statistic

$$\sum_i \frac{(F_i - F_{ith})^2}{F_{ith}} \tag{A4}$$

which should distribute like χ^2 for randomly drawn samples from a normal distribution, is then calculated from the real and ideal frequencies (F_i and F_{ith} respectively) and the values compared to the tabulated values of χ^2 at the relevant number of degrees of freedom, f, and desired confidence level. A value of $\Sigma\chi^2$ larger than the tabulated χ^2 is not likely to occur by chance (at 95% probability level) and results in a rejection of the hypothesis of normality of the variable ($\log l$).

Appendix 3. Determination of error in sample standard deviation

When a random sample is drawn from a population with a normal distribution with a variance σ^2, it is possible to make a statement on the variance of the sample (relative to that of the real population) as a function of sample size. For this, tables with the probability distribution of $\chi^2 = (s^2/\sigma^2)_n$ (as a function of n) are consulted. We have used this variance to arrive at a measure of the experimental error in the standard deviation of a sample of fibres.

With a sample size of n and a confidence level of 95% we can thus calculate the sample ratio s/σ as follows

$$P\left(\chi_1^2 \leq \frac{s^2}{\sigma^2} \leq \chi_2^2\right) = 0.95 \tag{A5}$$

χ^2 percentiles for low n can be found in statistic tables while for high n the following approximation can be used [17]

$$\chi_c^2 = f\left[1 - \frac{2}{9f} + z_c\left(\frac{2}{9f}\right)^{1/2}\right]^3 \tag{A6}$$

where z_c is the normal deviate at probability c (tabulated) and f is the number of degrees of freedom ($f = n - 1$).

For a sample size of $n = 110$ we arrive at

$$P\left(81.99 \leq \frac{s^2}{\sigma^2} \leq 118.43\right) = 0.95 \tag{A7}$$

giving

$$P\left[\left(\frac{81.99}{109}\right)^{1/2} \leq \frac{s}{\sigma} \leq \left(\frac{118.43}{109}\right)^{1/2}\right] = 0.95 \tag{A8}$$

which leads to

$$P\left(0.87 \leq \frac{s}{\sigma} \leq 1.13\right) = 0.95 \tag{A9}$$

which implies that the sample standard deviation will be at least 87% and not more than 113% of the population variance in 95% of the cases. In other words; the standard deviation (= width) of the real distribution will be within 13% of the measured sample standard deviation.

An estimation of the error in the width of the distribution with respect to the ideal log normal one can be made through estimation of the error in the peak height, df_{max}, of the relative frequency curve

$$f_{max} = \left(\frac{d\varphi}{d(\log x)}\right)_{max} = \frac{1}{\sigma(2\pi)^{1/2}} \tag{A10}$$

giving

$$\frac{df_{max}}{f_{max}} = -\sigma\, d\sigma \tag{A11}$$

Thus it is found that the relative error in the standard deviation is around 5%. This is within the range of the expected experimental error as discussed above.

References

1. P. KUMAR, K. VEDULA and A. RITTER (eds), "Processing and Properties for Powder Metallurgy Composites," Proceedings of TMS/AIME Symposium, Denver, CO (Metallurgical Society, 1987).
2. C. J. SKOWRONEK, A. PATTNAIK and R. K. EVERETT, "Dispersion and blending of SiC whiskers in RSP aluminium powders", Naval Research Laboratory NRL-MR-5750 (1986) p. 699.
3. M. McLEAN and R. DOWER, in "Proceedings of International Conference on Powder Metallurgy", Vol. 2, London, July 1990 (The Institute of Metals, London, 1990) p. 251.
4. J. H. ter HAAR and J. DUSZCZYK, *J. Mater. Sci.* **26** (1991) 3628.
5. *Idem., Mater. Sci. Engng* **A135** (1991) 65.
6. R. M. GERMAN, "Particle Packing Characteristics" (Metal Powder Industries Federation, New Jersey, 1989).
7. B. N. SINGH, *Powder Metall.* **14** (28) (1971) 277.
8. F. F. LANGE, L. ATTERAAS and F. ZOK *Acta Metall. Mater.* **39** (2) (1991) 209.
9. K. KAWAKITA and K. LÜDDE, *Powder Technol.* **4** (1970/71) 61.
10. P. J. JAMES, "Isostatic Pressing Technology" (Applied Science, London, New York, 1983).
11. R. L. HEWITT, W. WALLACE and M. C. de MALHERBE, *Powder Metall.* **17** (33) (1974) 1.
12. H. H. HAUSNER, *Int. J. Powder Metall.* **3** (4) (1967) 7.

13. M. C. KOSTELNIK and J. K. BEDDOW in "Modern Developments in Powder Metallurgy", Vol. 4, "Processes", edited by H. H. Hausner, Proceedings of the International PM Conference, July 1970, New York.
14. R. O. GREY and J. K. BEDDOW, *Powder Technol.* **2** (1968/1969) 323.
15. T. P. FISHER and D. S. COLEMAN, *Powder Metall.* **17** (34) (1974) 302.
16. H. F. FISCHMEISTER, E. ARZT and L. R. OLSSON, *ibid.* **4** (1978) 179.
17. H. B. CRAWFORD and B. E. ECKES (eds), "Perry's Chemical Engineers' Handbook" (McGraw-Hill, Singapore, 1984).

Received 4 September 1991
and accepted 17 February 1992